Electronic Supplementary Material (ESI) for RSC Advances.

Supporting Information

Layer-by-layer assembled polyaniline/carbon nanomaterials-coated cellulosic aerogel electrodes for high-capacitance supercapacitor applications

Shaoyi Lyu,[a,b*] Yanping Chen,[b,c] Shenjie Han,[b] Limin Guo, [b] Zhilin Chen, [b] Yun Lu,[b] Yuan Chen,[b] Na Yang[b] and Siqun Wang [d,b*]

[a] Research Institute of Forestry New Technology, Chinese Academy of Forestry, Beijing 100091, China.
[b] Research Institute of Wood Industry, Chinese Academy of Forestry, Beijing 100091, China.
[c] Beijing Engineering Research Center of Cellulose and Its Derivatives, School of Materials Science and Engineering, Beijing Institute of Technology, Beijing 100081, China.
[d] Center for Renewable Carbon, University of Tennessee, Knoxville, Tennessee, 37996, USA.

*Author for correspondence. Email: lvsy@caf.ac.cn (S. Lyu), swang@utk.edu (S. Wang).

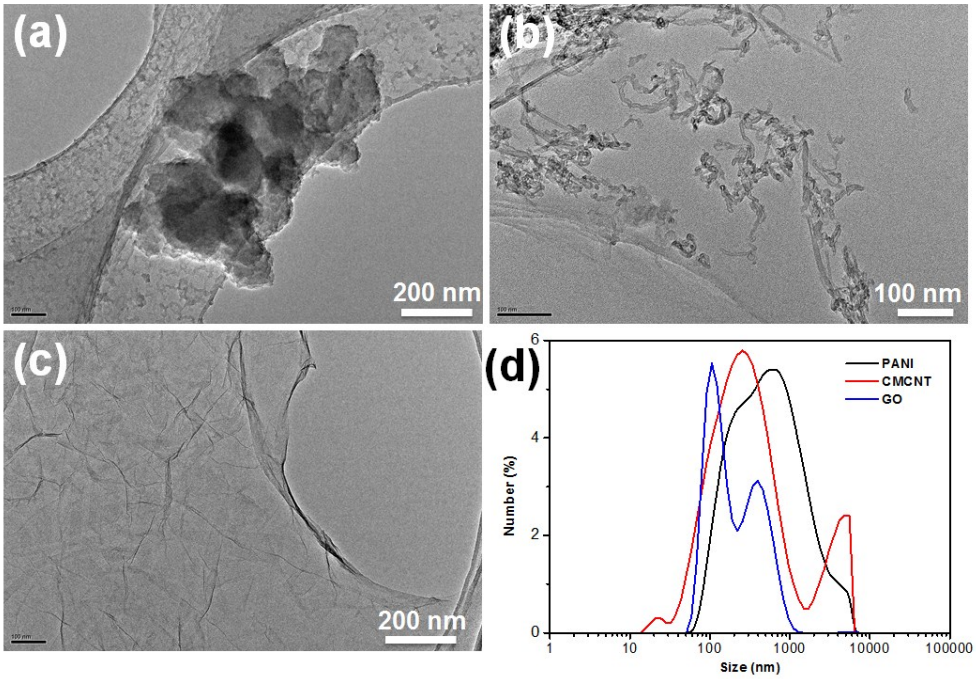

Figure S1. TEM images of (a) PANI, (b) CMCNT, and (c) GO. (d) Particle-size distributions of PANI, CMCNT, and GO.

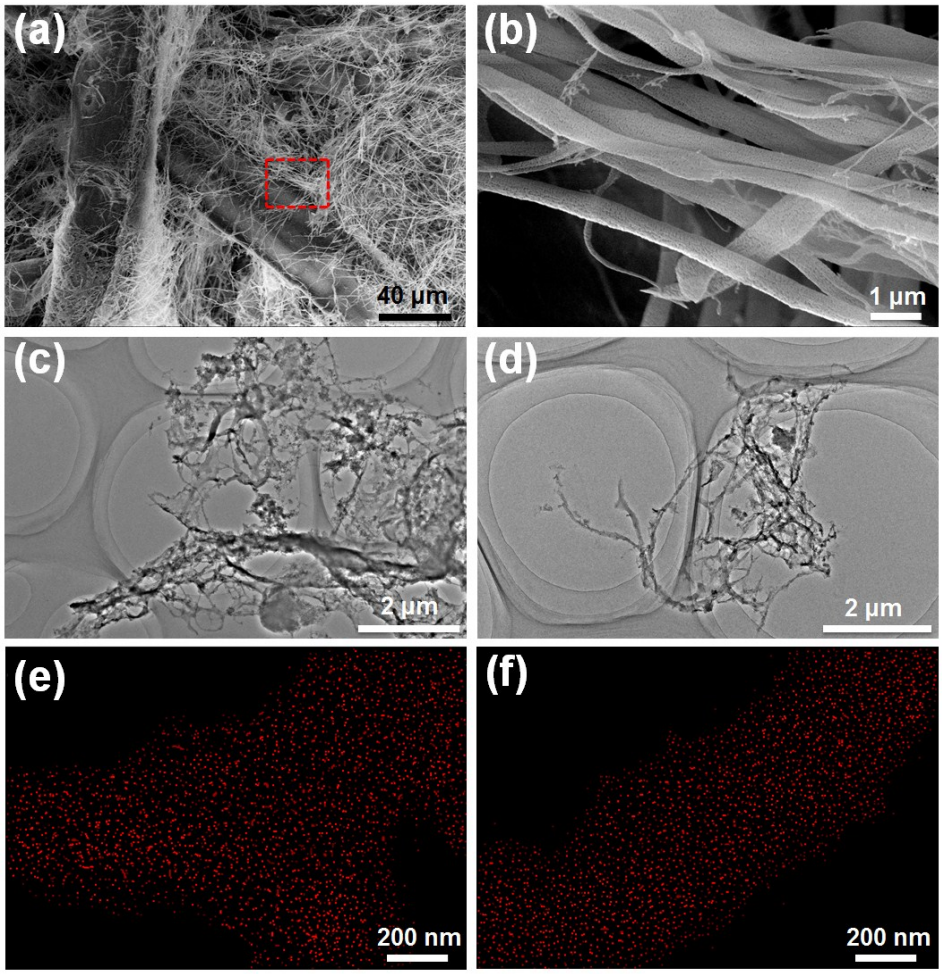

Figure S2. (a) SEM images of the WPF/CNC aerogel. (b) Enlarged SEM image of the section enclosed by the red dashed box in panel (a). TEM images of (c) 10 times LbL assembly of PANI/CMCNT and (d) PANI/GO on the nanofibers formed by CNC at a small magnification. Corresponding elemental mapping images of N from SEM/EDS image of (e) $(PANI/CMCNT)_{10}$ and (f) $(PANI/GO)_{10}$ on CNC nanofibres.

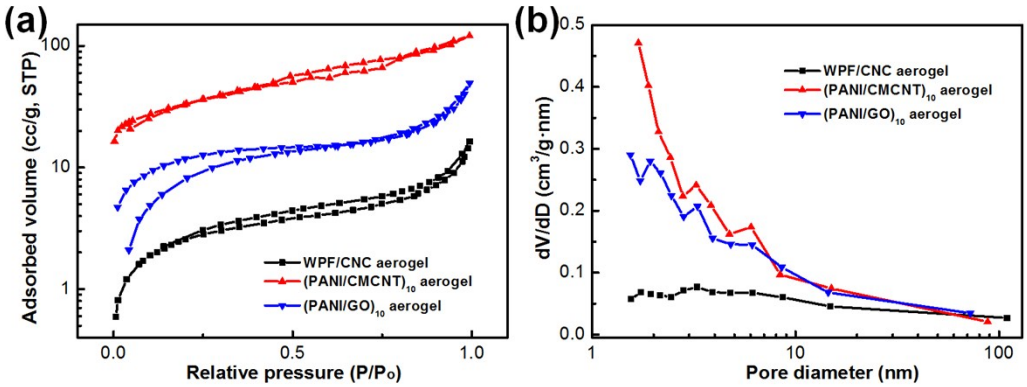

Figure S3. Typical nitrogen adsorption/desorption isotherms (a) and pore size distributions of the aerogels (b) for the WPF/CNC aerogel, the $(PANI/CMCNT)_{10}$ aerogel, and the $(PANI/GO)_{10}$ aerogel.

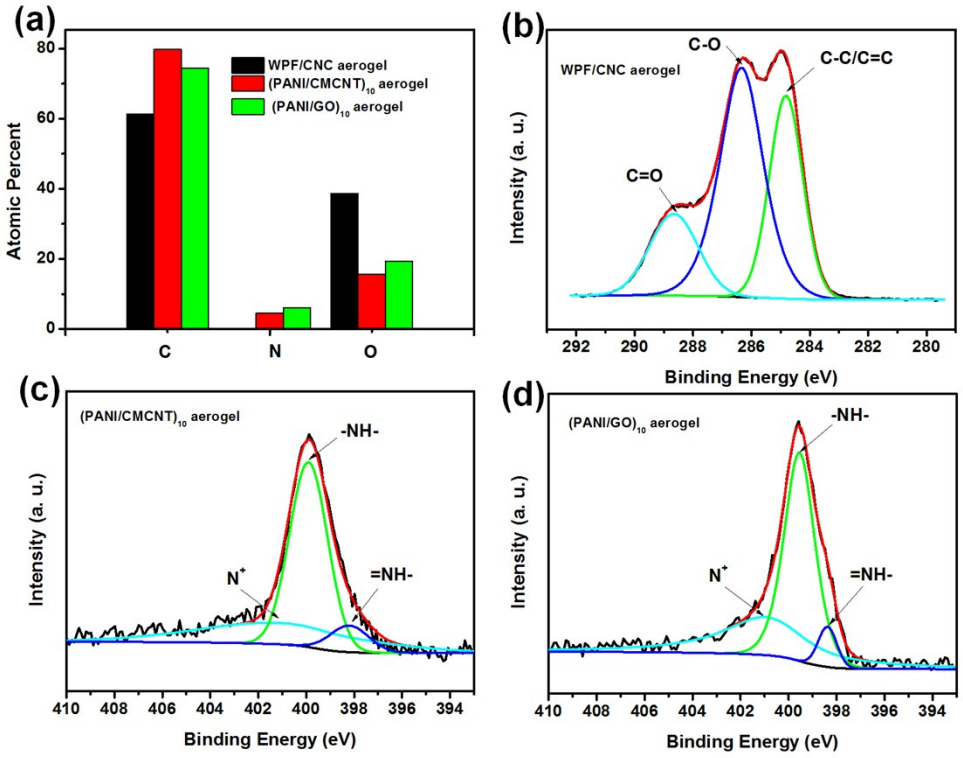

Figure S4. (a) Atomic percentages in the WPF/CNC, $(PANI/CMCNT)_{10}$, and $(PANI/GO)_{10}$ aerogels. (b) High-resolution XPS C1s spectrum of the WPF/CNC aerogel, and its deconvolution. High-resolution XPS N1s spectra of (c) the $(PANI/CMCNT)_{10}$ aerogel and (d) the $(PANI/GO)_{10}$ aerogel, and their deconvolutions.

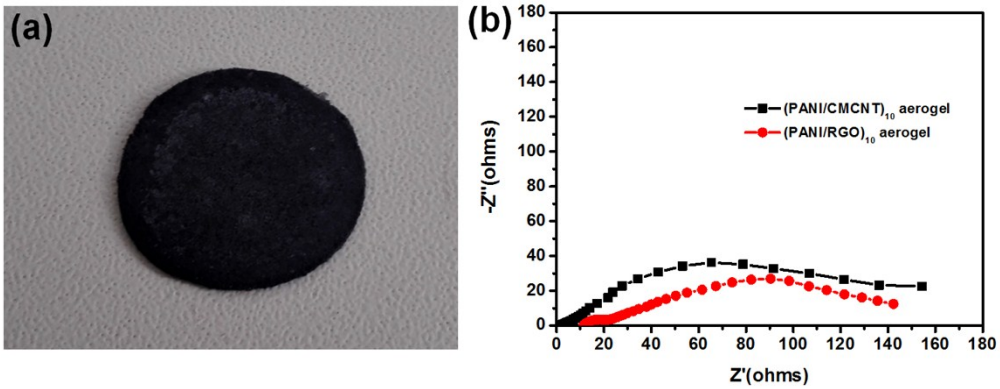

Figure S5. (a) Representative photographic image of a compressed aerogel film. (b) Nyquist plots for the $(PANI/CMCNT)_{10}$ and $(PANI/RGO)_{10}$ aerogel electrodes under three-electrode testing conditions.

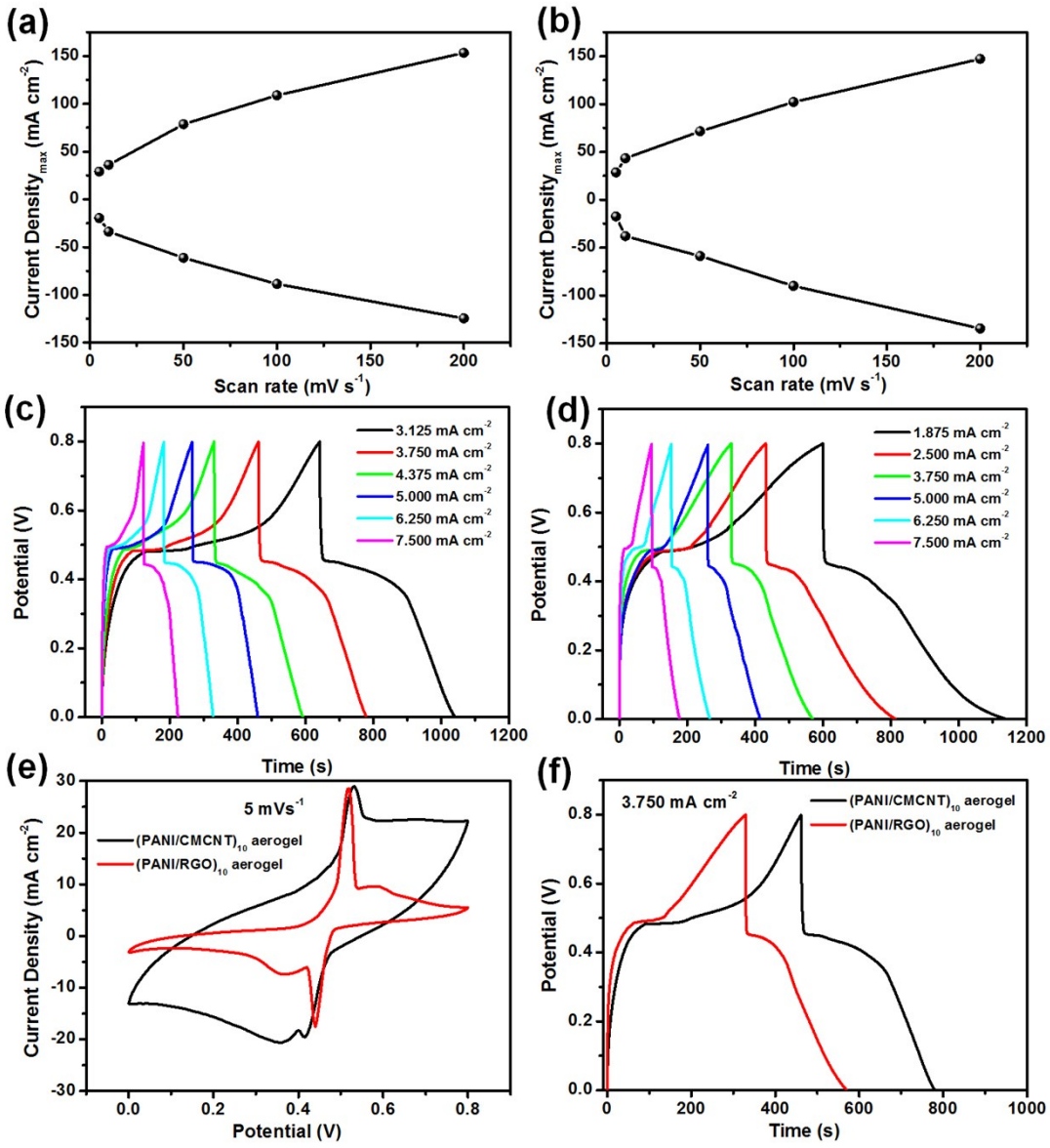

Figure S6. Maximum current vs. scan rate for (a) the $(PANI/CMCNT)_{10}$ and (b) the $(PANI/RGO)_{10}$ aerogel electrodes determined from their corresponding CV curves. GCD curves for (c) the $(PANI/CMCNT)_{10}$ and (d) the $(PANI/RGO)_{10}$ aerogel electrodes at different current densities. (e) CV curves for the $(PANI/CMCNT)_{10}$ and $(PANI/RGO)_{10}$ aerogel electrodes at a scan rate of 5 mV s^{-1}. (f) GCD curves of the $(PANI/CMCNT)_{10}$ and $(PANI/RGO)_{10}$ aerogel electrodes at a current density of 3.750 mA cm^{-2}. All data were acquired under three-electrode testing conditions.

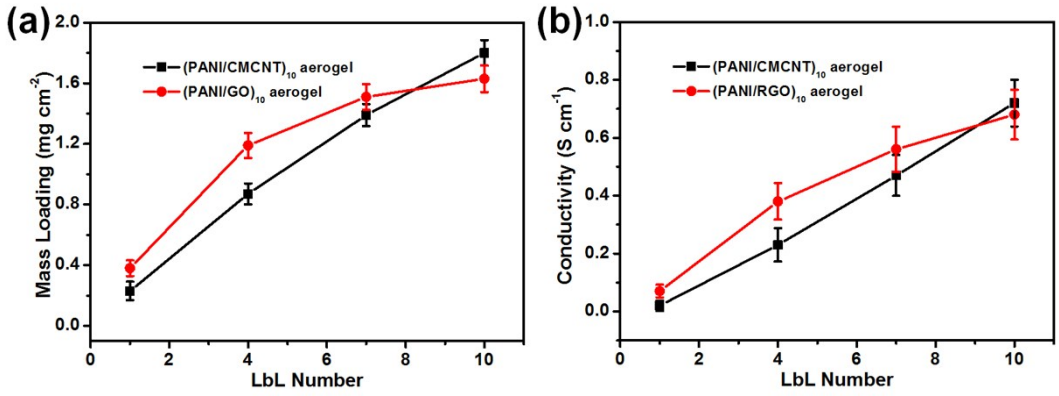

Figure S7. (a) Mass loadings and (b) conductivities of the $(PANI/CMCNT)_n$ and $(PANI/RGO)_n$ aerogels as functions LbL number.

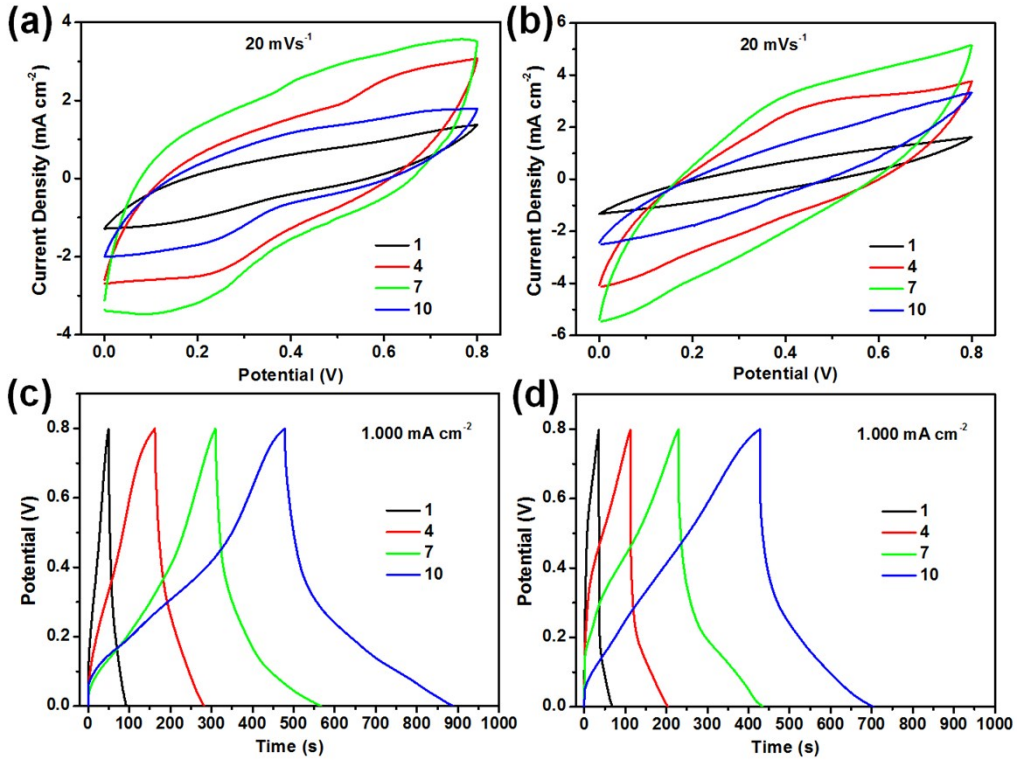

Figure S8. CV curves of the (a) $(PANI/CMCNT)_n$ and (b) $(PANI/RGO)_n$ aerogel electrodes acquired at a scan rate of 20 mV s^{-1} as functions of LbL number. GCD curves of (c) the $(PANI/CMCNT)_n$ and (d) $(PANI/RGO)_n$ aerogel electrodes at a current density of 1.000 mA cm^{-2} as functions of LbL number. All data were acquired under two-electrode testing conditions.

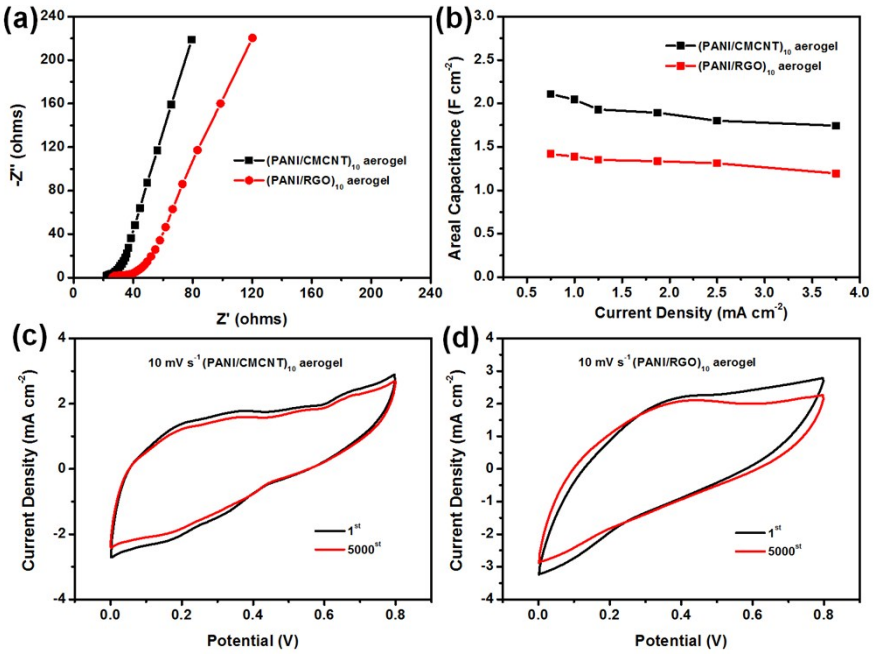

Figure S9. (a) Nyquist plots for the $(PANI/CMCNT)_{10}$ and $(PANI/RGO)_{10}$ aerogel electrodes. (b) Areal capacitances of the two aerogel electrodes at different current densities. CV curves for (c) the $(PANI/CMCNT)_{10}$ and (d) the $(PANI/RGO)_{10}$ aerogel electrodes during cycle-stability testing. All data were acquired under two-electrode testing conditions.

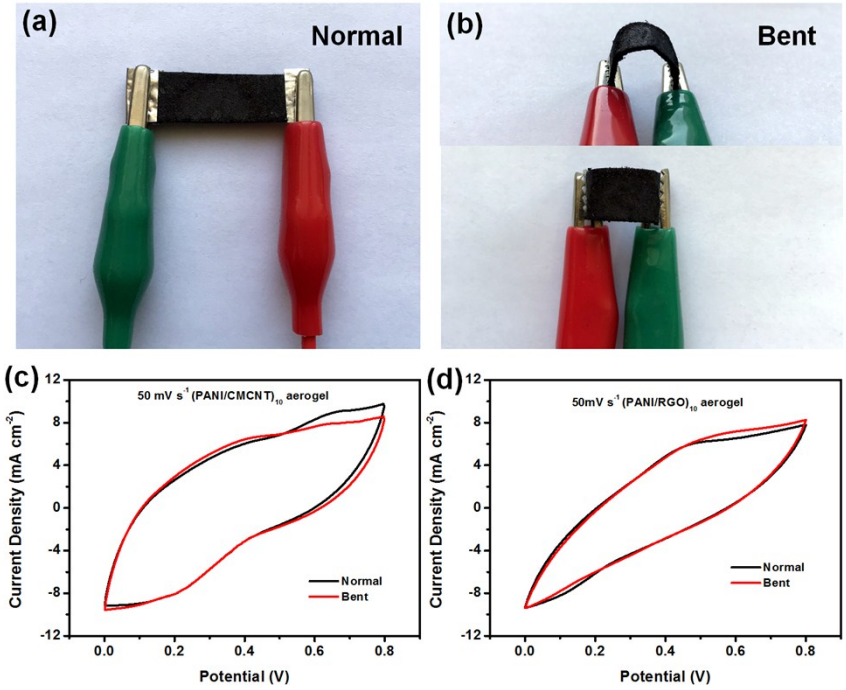

Figure S10. Representative photographic images of an electrode in its (a) normal and (b) bent state. CV curves of (c) the $(PANI/CMCNT)_{10}$ and (d) the $(PANI/RGO)_{10}$ aerogel electrodes during flexibility testing.